JAAS

Check for updates

Build-a-bone: development of a matrix-matched reference material for quantitative analysis of bone with portable LIBS

Kristen M. Livingston, [iD] ab Amanda T. Williams [iD] ab and Matthieu Baudelet [iD] *abcd

With the rising popularity of laser-induced breakdown spectroscopy (LIBS) for studying skeletal samples, the need for a matrix-matched reference material for quantitative analysis of bone has become a priority. Previous calibration materials used for laser-based sampling include glass standards, bone powders, carbonates, and hydroxyapatite standards, all of which fail to imitate both the physical and the chemical properties of the matrix of bone samples. This study focuses on the development, characterization, and application of matrix-matched reference material for bone. These materials are composed of a compact collagen scaffold that is embedded with elementally-enriched hydroxyapatite crystals. Physical characterization of the composites indicates a hydroxyapatite crystallinity and pore size that corresponds to bone. Molecular characterization confirms the presence of hydroxyapatite and collagen throughout the material, while elemental analysis reveals a profile nearly identical to that of bone. Calibration curves for strontium and barium were developed for portable LIBS (pLIBS) analysis, finding limits of detection and quantification values of 123 $\mu g\ g^{-1}$ and 140 $\mu g\ g^{-1}$ for strontium, and 29 $\mu g\ g^{-1}$ and 37 $\mu g\ g^{-1}$ for barium. Validation was performed on bone fragments for which pLIBS signal was used to determine the concentration of strontium and barium.

1. Introduction

1.1. Laser ablation analysis of bone

Laser-induced breakdown spectroscopy (LIBS) has become an increasingly popular analytical tool for the chemical analysis of bone. The minimal sample preparation, *in situ* micro-destructive sampling, and rapid acquisition time are advantageous aspects of LIBS analysis. It is used to determine the elemental composition of bone across a wide range of applications, from forensic investigation, biomedical research, environmental studies, and bioarchaeological explorations.[1–8] These elemental profiles may help provide contextual understanding about the skeletal samples. For example, the presence of trace elements, such as lead, has been studied in relation to

aDepartment of Chemistry, University of Central Florida, USA. E-mail: baudelet@ucf.edu

bNational Center for Forensic Science, University of Central Florida, USA

cCREOL – the College of Optics and Photonics, University of Central Florida, USA

dDepartment of Anthropology, University of Central Florida, USA

Kristen Livingston is a Chemistry PhD candidate at the University of Central Florida in Orlando, Florida. After working as an undergraduate researcher at the University of South Carolina analyzing spectroscopic variations of dyed fibers, she decided to pursue a PhD in analytical chemistry that focused on forensic applications. Kristen's dissertation research, which is conducted at the National Center for Forensic Science, focuses on the analysis of skeletal remains using Laser-induced Breakdown Spectroscopy (LIBS). Most notably, her work demonstrates how the elemental profile of skeletal remains functions as a potential tool for the reassociation of commingled remains. She is also working towards the creation of matrix-matched calibration standards for quantitative analysis of bone. After working in a niche field that sits at the intersection of chemistry, anthropology, statistics, and forensic science, Kristen is a supporter of interdisciplinary studies that push the boundaries of spectroscopy research. She has had incredible opportunities to travel the world to places like Romania and Hawaii to analyze samples and is very excited to see where her career takes her next.

Kristen M. Livingston

medical diagnostics.[2,9] Strontium and barium are common dietary indicators in bioarcheological reconstructions.[3,10] Elemental variation due to diagenetic alterations occurring after death have also been evaluated.[4,11] LIBS profiles of human skeletal remains have even been assessed as a possible means for reassociating commingled remains in forensic contexts.[7,8,12]

LIBS analysis of skeletal remains has also become more practical with the commercial availability of portable LIBS (pLIBS) instrumentation. Field-deployable instruments enable analysts to travel between field sites and laboratories to examine samples. Another benefit of pLIBS is the ability to analyze whole, intact bone samples that would otherwise need to be destructively sampled to fit within a LIBS sample chamber. This is critical for the study of forensic and bioarcheological settings where samples are often limited, or invasive sampling techniques are discouraged. The ease and accessibility of LIBS for skeletal samples make it a great qualitative technique. However, one primary analytical challenge that has yet to be solved is the development of a matrix-matched standard that supports quantitative, laser-based analysis of bone.

1.2. The need for matrix-matched standards

Despite the lack of an ideal reference material for bone, a number of quantitative laser-ablation studies of bone have been published.[5,6,13–16] Calibration approaches in such works include the use of certified reference materials, including trace elements in glass (NIST6XX series) and bone meal/bone ash powders (NIST1486 and NIST1400). Other reference standards have included lab-synthesized hydroxyapatite pellets and calcium carbonates. None of these standards can provide effective quantitative results for LIBS because they (1) fail to fully match the chemical composition of bone, (2) lack the physical composition of bone necessary to ensure reproducible laser–sample interactions, or (3) cannot provide a multi-point calibration curve necessary for reliable quantitation. With the growing field of research for LIBS applications to skeletal samples, the development of reference material suitable for laser ablation of bone is a vital necessity.

1.3. Composition of bone to be simulated in reference materials

Matrix-matching for laser-based sampling requires imitating both the chemical and physical properties of the sample. For skeletal samples, the goal is to replicate the compact, outer layer of bone known as cortical bone. Cortical bone tissue is composed of collagen fibrils, embedded with hydroxyapatite, $Ca_5(PO_4)_3OH$, crystals.[17,18] These mineralized fibrils are arranged in close-packed fiber arrays, known as lamellae, which are further organized into the structural units of cortical bone tissue known as osteons. The highly ordered arrangement of osteons in bone creates a dense physical structure, with small pores that allow for blood flow, nutrient diffusion, and movement of bone cells.[19,20] The major components of collagen and hydroxyapatite have a mass percent of roughly 30% organic material and 70% inorganic mineral. Minor and trace elements found in bone are predominantly found in hydroxyapatite, as

these elements substitute in for Ca^{2+}, PO_4^{3-}, or OH^- ions or reside within interstitial spaces of lattice.[21,22] Commonly known minor and trace elements in bone include Na, K, Mg, Sr, Ba, Fe, Zn, and Al.

The matrix of a bone reference material is expected to mimic the bulk chemical composition of bone, while also possessing a compact structure that retains a porosity. Additionally, the materials must allow for controllable, trace elemental incorporations across a range of calibrations to ensure multi-point calibration curves. This research study proposes a synthetic material designed to imitate cortical bone that can be doped with trace elements and used to calibrate portable LIBS signal for the quantitative analysis of bone.

2. Materials and methods

2.1. Synthesis and spiking of hydroxyapatite

A range of matrix-matched scaffolds were prepared via a co-precipitation method combining synthesized hydroxyapatite and insoluble collagen, adapted from previous studies.[23–25] The scaffolds were spiked utilizing strontium (Sr) and barium (Ba) elemental standards (SCP Science, Quebec, Canada).

For the synthesis of hydroxyapatite (HAP), equal volumes of calcium nitrate tetrahydrate ($Ca(NO_3)_2·4H_2O$, 1.0 M; VWR International, Radnor, PA) and ammonium dihydrogen phosphate ($NH_4H_2PO_4$, 0.6 M; VWR International, Radnor, PA) were mixed separately. Ammonium hydroxide (NH_4OH; Acros Organics, Fair Lawn, NJ) was used to adjust the pH of each solution to a pH of 10. To create doped HAP powder, Sr and Ba were added to the calcium nitrate solution at increasing concentrations and the calcium nitrate solution was added dropwise to the ammonium phosphate solution at a rate of 6 mL min^{-1}. The mixture was covered and placed in an orbital shaker for 3 hours, then left to age for 48 hours at room temperature. The precipitate was filtered and calcined at 450 °C for 3 hours in a muffle furnace. The amalgamate was then ground to a fine powder.

2.2. Creation of collagen-hydroxyapatite composites/pellets

A 3% w/v solution consisting of Type I bovine collagen (COL; Sigma-Adrich, St. Louis, MO) and 5 mM hydrochloric acid (HCl; Sigma-Aldrich, St. Louis, MO) was left to swell overnight at 48 °C. After centrifuging, the supernatant was discarded, and the product was reconstituted with 5 mM HCl and vortexed. While stirring the collagen slurry, the synthesized hydroxyapatite powder was added at a 30 : 70 COL : HAP ratio by weight. To ensure crosslinking of collagen fibrils, 15 mM n-hydroxysuccinimide (NHS; Sigma-Aldrich, St. Louis, MO) and 30 mM n-(3-dimethylaminopropyl)-n′ ethylcarbodiimide hydrochloride (EDC; Sigma-Aldrich, St. Louis, MO) were added. Resulting solutions were added to 3 mm × 10 mm cylindrical molds and placed in a −30 °C freezer for 24 hours. After removing, the mold was placed under vacuum to dry. The scaffolds were then pelletized using a manual arbor press.

This journal is © The Royal Society of Chemistry 2025

J. Anal. At. Spectrom., 2025, **40**, 3184–3191 | 3185

2.3. Characterization of pellets

2.3.1 Physical (digital microscopy). After pressing the pellets, images were acquired at 20×, 200×, and 500× using a digital microscope (VHX-6000, Keyence Corp., Itasca, IL).

2.3.2 Molecular (XRD, ATR-FTIR). After the synthesized hydroxyapatite sample was ground, analysis was performed by X-ray diffraction (Empyrean, Malvern Panalytical Ltd, Malvern, UK) and the High Score software package with ICDD database. Scans were done between 2θ of 10°–80° with a resolution of 0.05° using the Cu K-alpha X-ray emission wavelength (1.54 Å). Attenuated total reflection Fourier-transform infrared spectroscopy was performed on the pressed pellet as well as milled bovine bone powder (Spectrum Two FTIR Spectrometer, PerkinElmer, Waltham, MA) with the Spectrum 10 software. Results were averaged from sixteen scans at a resolution of 4 cm^{-1}. Multiple spectra were taken on each sample to ensure a representative signal was obtained.

2.3.3 Elemental (pLIBS, ICP-MS). Pressed pellet samples were analyzed using portable LIBS (pLIBS) (SciAps Z-300, SciAps Inc., Andover, MA) and Profile Builder software. Small fragments of bovine marrow bone were also analyzed by pLIBS as validation samples. The Z-300 is equipped with a 1064 nm Nd : YAG laser with laser energy of 5 mJ. (The fluence of the laser in this instrument cannot be adjusted, as both laser energy and spot size are predetermined.) Each sample spectrum was acquired at a 50 Hz pulse rate, with the three-channel spectrometer (190 to 950 nm) set at a 292 ns gate delay with 1 ms integration time. Multiple sample locations on each pellet (5 locations) and bone fragments (3 locations) were analyzed; each sampling consisted of 3 cleaning shots followed by 12 data shots. Prior to further analysis, all LIBS spectra are normalized to the non-resonant Ca I line at 442.6 nm to ensure fluctuations are representative of the matrix itself rather than plasma conditions.

Pellets and bone fragments were digested with trace-metal grade nitric acid (HNO$_3$; ThermoFisher Scientific, Waltham, MA) in the Multiwave 5000 (Anton Paar, Graz, Austria) with a 20SVT50 rotor. Samples were diluted with 18.2 MΩ cm^2 ultrapure water and spiked with an indium internal standard before being introduced to the PlasmaQuant Elite ICP-MS (AnalytikJena, Jena, Germany) using the AspectMS software package.
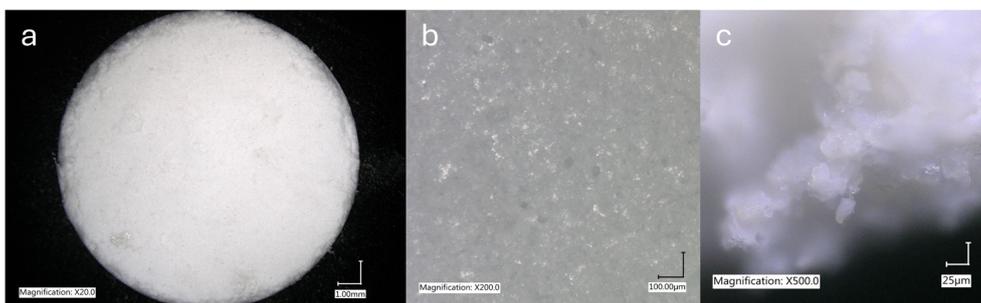

Fig. 1 Digital micrographs of synthesized reference material. (a) Overview of HAP–COL pellet. (b) Pores produced by crosslinking of collagen fibrils. (c) Hydroxyapatite crystals trapped within collagen framework of pellet.
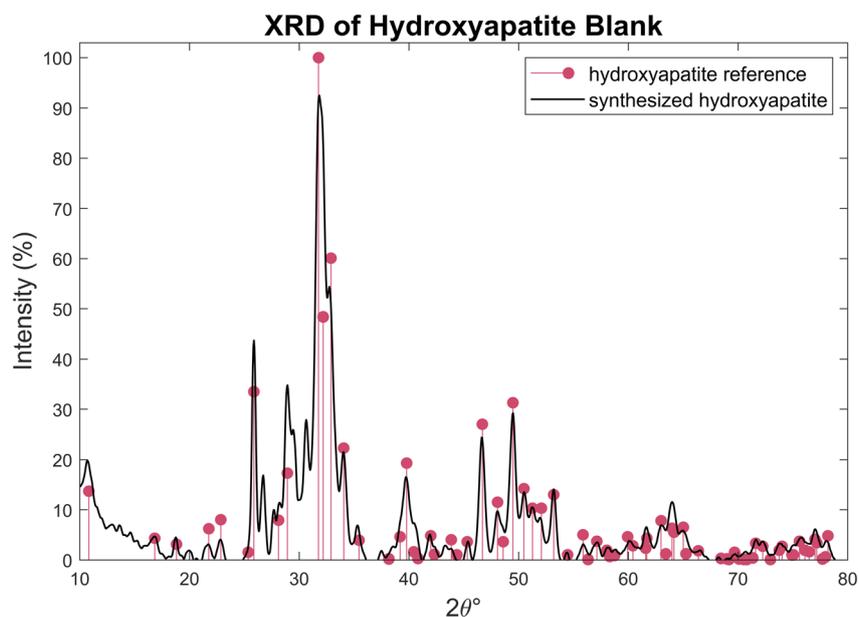

Fig. 2 XRD comparison of synthesized hydroxyapatite with reference spectrum.

3186 | *J. Anal. At. Spectrom.*, 2025, **40**, 3184–3191

This journal is © The Royal Society of Chemistry 2025

All spectral processing, visualization, and analyses were performed using MATLAB software (MathWorks, Natick, MA).

3. Results and discussion

3.1. Physical characterization

3.1.1 Digital microscopy. Micrographs of the outer surface of the pellet and its cross-section reveal the presence of a compact yet porous collagen framework containing mineral crystals (Fig. 1a–c). Each pellet measures approximately 13 mm in diameter with a thickness of 2.76 mm (see SI). While compact and dense, the pellet still maintains a visible level of porosity. The diameter of the pores range from approximately 0.78 μm to 175 μm, imitating the reported pore size in cortical bone of 50 μm to 250 μm.[26,27] The grain sizes of HAP crystals found within the pellet are measured between 13.4 μm to 98.1 μm. Due to the agglomeration of hydroxyapatite particles, this granularity is larger than that of individual crystals in bone.[28] However, the

presence of large particles within the pellets simulates the close packing of mineralized fibril arrays present in cortical bone.

3.2. Crystalline and molecular characterization

3.2.1 XRD. The crystalline structure of the lab-synthesized hydroxyapatite, prior to elemental spiking, was evaluated by XRD. The powder XRD spectrum of the product is shown in Fig. 2 with a reference spectrum for hydroxyapatite derived from Rodriguez, et al.[29] The alignment of the experimental and reference spectra confirms the presence of hydroxyapatite, rather than another apatite or calcium phosphate mineral. The average crystalline size of the hydroxyapatite powder was calculated to be approximately 65.2 nm, based on the Scherrer Method.[30,31] This is consistent with the range of reported hydroxyapatite particle dimensions of 50 nm to 100 nm in length and 30 nm to 50 nm in width, with a thickness of 2 nm to 6 nm.[28]

3.2.2 FTIR. The molecular composition of the collagen-hydroxyapatite composite pellet was analyzed and compared
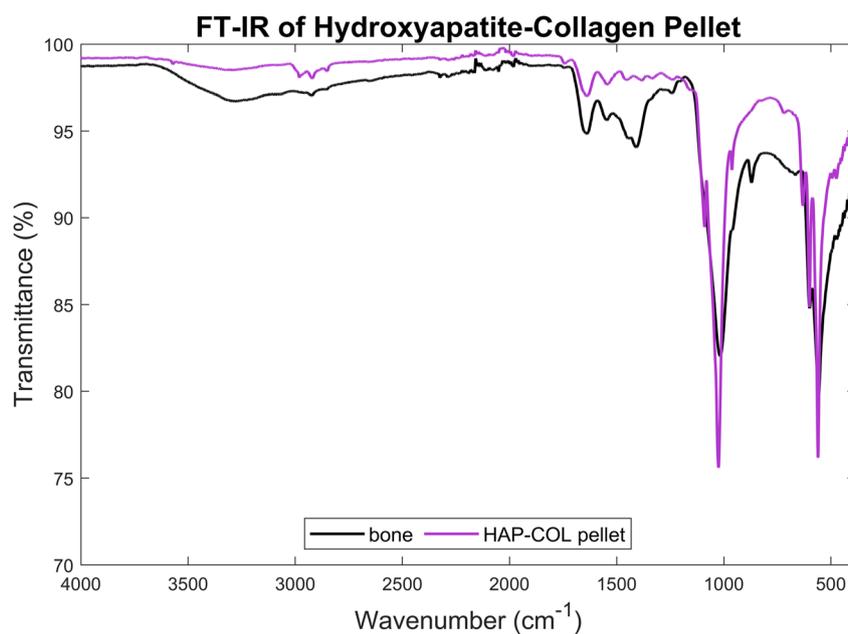

Fig. 3 Molecular comparison of HAP-COL pellet with bovine bone powder using ATR-FTIR.

Table 1 Assignment of functional groups in FT-IR of synthesized reference materials

Wavenumber (cm^{-1})	Functional group	Structural characteristic
560 and 601	Phosphate (PO_4^{3-})	Bending (v4) of P–O
631	Hydroxyl (–OH)	Wagging of O–H
720	Amide IV	Bending of N–H
962	Phosphate (PO_4^{3-})	Symmetric stretching (v1) of P–O
1025 and 1092	Phosphate (PO_4^{3-})	Asymmetric stretching (v3) of P–O
1239, 1382, and 1455	Amide III	Stretching of N–H and bending of C–N
1545	Amide II	Stretching of N–H and bending of C–N
1640	Amide I	Stretching vibration of C=O
2851, 2921, and 2981	Amide B	Stretching vibration of C–H
3296	Amide A	Stretching vibration of N–H
3571	Hydroxyl (–OH)	Stretching vibration of O–H

This journal is © The Royal Society of Chemistry 2025

J. Anal. At. Spectrom., 2025, **40**, 3184–3191 | **3187**

to that of bovine cortical bone (Fig. 3). Key molecular signals from both collagen and hydroxyapatite are summarized in Table 1, based on previous research studies.[32–35]

Discrepancies in intensity can be seen in the Amide A and Amide III regions, where the reference material has a lower absorbance. This could be attributed to a lower collagen content in the HAP-COL pellet than in bone, though it is more likely the result of an increased transmittance through the collagen in the pellet, due to its porous framework. The ATR-FTIR spectrum also reveals that the phosphate vibrational modes in the reference material are slightly more intense, sharper, and more distinct than the broadened signal from milled bone. The improvement in signal in the reference material results from the larger surface area of HAP crystals present in the pellet. Observed differences between the synthesized reference material and bone reference result from the physical, not chemical, differences between a pressed solid and a powder. Overall, there is an overwhelming similarity in molecular profiles between the synthesized calibration standard and a true bone, which supports the objective of chemical matrix-matching.

3.3. Elemental characterization

3.3.1 LIBS comparison of blank pellet to bone sample. The non-doped HAP-COL pellet and bovine bone fragments were analyzed by portable LIBS and compared to evaluate similarities in elemental profile (Fig. 4). The overlap in optical emission profiles between the HAP-COL pellet and bone establishes that the elemental composition of the lab-synthesized pellets mimics bone. The LIBS profiles of the pellet show signal from both the organic (C and N) and inorganic (Ca and P) components necessary for accurate matrix-matching. Similarities in

the spectral emissions also indicate that the physical composition of the pellet produces a LIBS signal representative of bone. The observable differences between spectra are at emission lines of minor elements Mg, K, Na, and Sr, at which the reference blank has a significantly lower signal due to no targeted incorporation of these elements.

3.3.2 ICP-MS cross-validation of spikes. Nominal concentrations of trace elements were selected to create a linear calibration model in the range that covers the elemental levels in bone reported in literature.[36] ICP-MS was used to measure the incorporation of both Sr and Ba within the pellets, compared to the initial spiked amounts (Table 2).

Estimated recovery for strontium and barium spikes are around 50% (see SI). This yield can likely be attributed to loss of analytes during the precipitation, filtering, and calcination

Table 2 Concentration of Sr and Ba in reference materials, obtained by ICP-MS. The errors are 1σ values measured in replicate samples

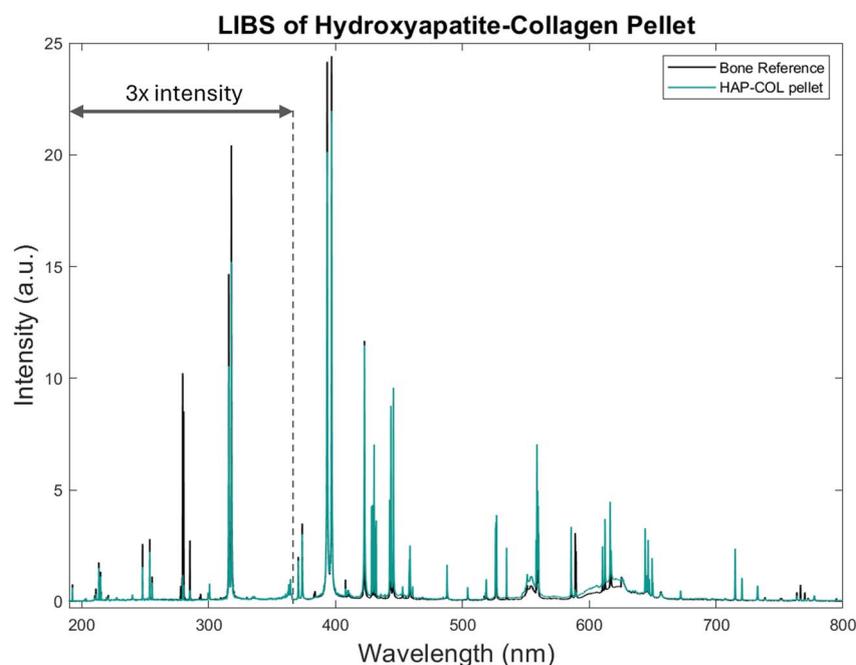| Standard	Nominal concentration ($\mu g\ g^{-1}$)	Element	ICP-MS concentration ($\mu g\ g^{-1}$)
S1	0	Sr	103.22 ± 0.84
		Ba	19.74 ± 1.21
S2	50	Sr	158.60 ± 1.46
		Ba	54.55 ± 1.35
S3	100	Sr	172.71 ± 1.83
		Ba	74.02 ± 1.29
S4	200	Sr	217.93 ± 1.03
		Ba	125.53 ± 2.35
S5	400	Sr	324.18 ± 3.08
		Ba	233.85 ± 3.86

Fig. 4 Spectral comparison of the elemental emission profiles of HAP-COL pellets and bovine marrow bone obtained by portable LIBS. The UV spectral region is amplified for clarity.
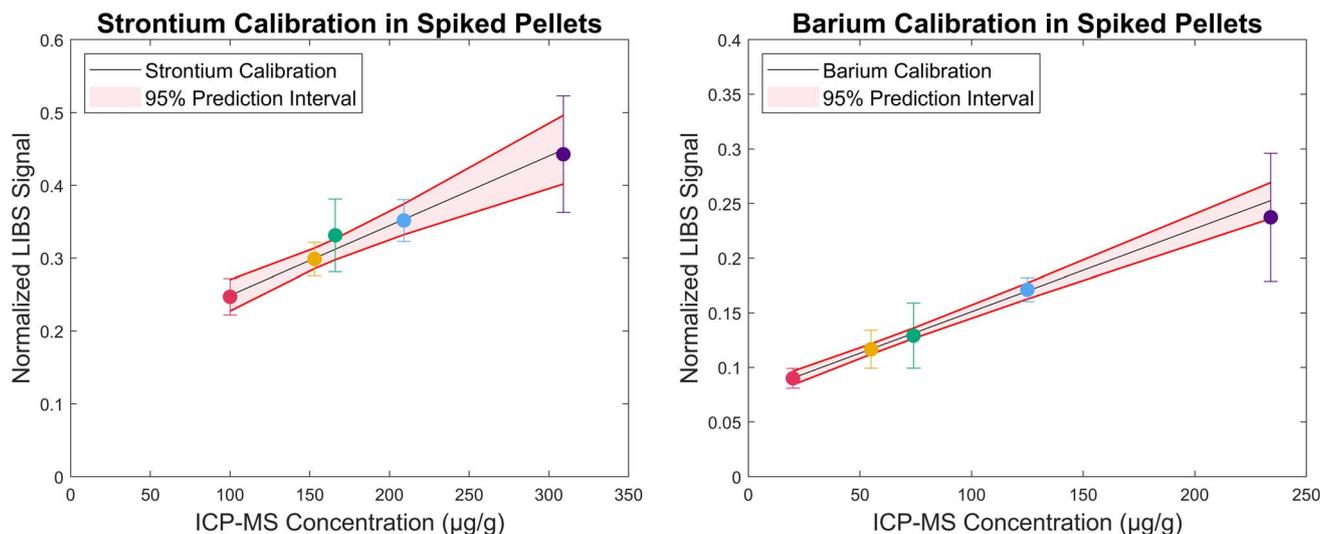
3188 | J. Anal. At. Spectrom., 2025, **40**, 3184–3191

This journal is © The Royal Society of Chemistry 2025

Fig. 5 Portable LIBS calibration curves for strontium and barium created using the synthetic HAP-COL reference standards; 95% confidence prediction bands are shaded in red.

processes of hydroxyapatite synthesis. The elevated Sr in each standard can be attributed to the presence of strontium in starting reagents, given the notable Sr concentration within the reference blank.

3.3.3 Portable LIBS calibration. The presence of trace elemental emission lines in each standard was evaluated using portable LIBS. The normalized LIBS signal reveals an increase in emission intensity with increasing concentration for each element. The corresponding wavelengths selected for calibration are Sr I line 460.8 nm and the Ba II line at 455.6 nm (see SI). Fig. 5 shows the LIBS calibration curves for each element. The limit of detection and limit of quantitation were determined following the method outlined by Mermet.[37] Limits of detection (LOD) and limits of quantitation (LOQ) by the pLIBS were calculated for both elements. The LOD and LOQ for strontium, respectively, are 123 $\mu g\ g^{-1}$ and 140 $\mu g\ g^{-1}$; barium signal resulted in an LOD of 29 $\mu g\ g^{-1}$ and LOQ of 37 $\mu g\ g^{-1}$.

The relatively high LOD and LOQ values for strontium are primarily the result of the elevated levels of Sr in the non-doped reference material, at over 100 $\mu g\ g^{-1}$. The use of higher purity reagents would improve this by reducing initial Sr concentrations. The barium calibration is seen to exhibit much lower detection and quantitation limits, reflecting values of barium that are likely to be found in bone. Nonetheless, these analytical

values of merit are ultimately limited by the sensitivity of the pLIBS, where the signal-to-noise ratio is low for elements with concentrations below 30 $\mu g\ g^{-1}$.[38] Despite this, these HAP-COL standards remain useful for bone samples with concentrations of Sr above 140 $\mu g\ g^{-1}$ and Ba above 37 $\mu g\ g^{-1}$.

3.3.4 Testing calibration standards with bone samples. Quantitative analysis of bone samples was performed using pLIBS and the synthesized reference materials and further validated by subsequent ICP-MS quantitation. It should be noted that this comparison illustrates the general application of HAP-COL standards for bone and is not intended to represent forensic or bioarchaeological analysis of bones.

Strontium and barium were both detected and quantified in the two bone fragments used as validation samples. Table 3 shows the values measured by ICP-MS, which serves as a cross-validation technique, alongside the concentrations determined by Sr and Ba signals from pLIBS of the bones. While the spectra from Bone 1 resulted in an overestimation of concentrations, Bone 2 represents successful quantitation by LIBS. In Bone 2, the expected sample concentrations for Sr and Ba are within 1σ of the value determined by LIBS.

4. Conclusion

As the increasing need for quantitative analysis of bone materials has been demonstrated by the existing published research, the results of this research study reveal that critical steps are being made towards a more reliable, matrix-matched reference material for bone. A compact pellet composed of collagen and hydroxyapatite and exhibiting the porosity and crystallinity of cortical bone was successfully synthesized. Molecular and elemental characterization demonstrated the chemical similarity of the synthetic reference material to bone. A range of calibration materials were created through controlled elemental spiking from 0 $\mu g\ g^{-1}$ to 250 $\mu g\ g^{-1}$, which were used to

Table 3 Quantitative comparison between pLIBS and ICP-MS on bone samples. Uncertainties are determined by the 1σ standard deviation of replicate sample measurements

	Sr ($\mu g\ g^{-1}$)		Ba ($\mu g\ g^{-1}$)	
Sample	ICP-MS	pLIBS	ICP-MS	pLIBS
Bone 1	255.3 ± 2.0	370.3 ± 98.6	59.3 ± 1.4	95.1 ± 20.8
Bone 2	249.0 ± 2.1	220.4 ± 28.4	56.1 ± 0.8	50.5 ± 22.4

This journal is © The Royal Society of Chemistry 2025

J. Anal. At. Spectrom., 2025, **40**, 3184–3191 | **3189**

effectively quantify the strontium and barium content in a real-world bone sample within 1σ of the accepted value. While the reference materials developed in this study show an advancement in the ability to conduct quantitative LIBS on bones, the experimental results are hindered primarily by the sensitivity of portable LIBS analyzers. Future goals include the use of higher sensitivity LIBS instrumentation as well as LA-ICP-MS for demonstrating LOD and LOQ values attainable with other laser-ablation-based analysis. An increased sensitivity could also enable detection of a broader range of elements such as copper, zinc, manganese, and lead that are often present in trace concentrations in bone.[36,39,40] This study is a stepping-stone for the development of analytical standards reproducing the physical and chemical characteristics of osseous materials, which opens a new area of quantitative analysis in biomedical, forensic, and anthropological studies.

Author contributions

Conceptualization (K.M.L.), data curation (K.M.L., M.B.), formal analysis (K.M.L., A.T.W., M.B.), funding acquisition (M.B.), investigation (K.M.L., A.T.W), methodology (K.M.L.), visualization (K.M.L.), writing – original draft (K.M.L., A.T.W.), writing – review & editing (all authors).

Conflicts of interest

There are no conflicts of interest to declare.

Data availability

Data for the results in this study are not publicly available at this time but may be obtained from the authors upon reasonable request until availability *via* the University of Central Florida Showcase of Text, Archives, Research & Scholarship (STARS). Supplementary information is available. See DOI: https://doi.org/10.1039/d5ja00209e.

Acknowledgements

References

1 M. A. Kasem, J. J. Gonzalez, R. E. Russo and M. A. Harith, LIBS analysis of artificial calcified tissues matrices, *Talanta*, 2013, **108**, 53–58, DOI: 10.1016/j.talanta.2013.02.062.

2 A. Shahedi, E. Eslami and M. R. Nourani, Influence of Lead on the Interpretation of Bone Samples with Laser-Induced Breakdown Spectroscopy, *J. Spectrosc.*, 2016, **2016**(1), 8205479, DOI: 10.1155/2016/8205479.

3 M. A. Kasem, J. J. Gonzalez, R. E. Russo and M. A. Harith, Effect of the wavelength on laser induced breakdown spectrometric analysis of archaeological bone, *Spectrochim. Acta, Part B*, 2014, **101**, 26–31, DOI: 10.1016/j.sab.2014.07.010.

4 X. Bai, A. Pin, J. Lin, M. Lopez, C. Koch Dandolo, P. Richardin and V. Detalle, The first evaluation of diagenesis rate of ancient bones by laser-induced breakdown spectroscopy in archaeological context prior to radiocarbon dating, *Spectrochim. Acta, Part B*, 2019, **158**, 105606, DOI: 10.1016/j.sab.2019.04.007.

5 O. Samek, D. C. S. Beddows, H. H. Telle, J. Kaiser, M. Liška, J. O. Cáceres and A. Gonzáles Ureña, Quantitative laser-induced breakdown spectroscopy analysis of calcified tissue samples, *Spectrochim. Acta, Part B*, 2001, **56**(6), 865–875, DOI: 10.1016/S0584-8547(01)00198-7.

6 G. D. Al-Khafif and R. El-Banna, Reconstructing Ancient Egyptian Diet through Bone Elemental Analysis Using LIBS (Qubbet el Hawa Cemetery), *BioMed Res. Int.*, 2015, **2015**, 281056, DOI: 10.1155/2015/281056.

7 K. M. Livingston, K. Zejdlik and M. Baudelet, Reassociation of Skeletal Remains Using Laser-Induced Breakdown Spectroscopy, *Anal. Chem.*, 2024, **96**(23), 9478–9485, DOI: 10.1021/acs.analchem.4c00876.

8 K. Kuehn, K. M. Livingston, J. D. Bethard and M. Baudelet, Association of commingled human skeletal remains by their elemental profile using handheld laser-induced breakdown spectroscopy, *Forensic Sci. Int.*, 2025, **367**, 112312, DOI: 10.1016/j.forsciint.2024.112312.

9 J. Rodríguez and P. M. Mandalunis, A Review of Metal Exposure and Its Effects on Bone Health, *J. Toxicol.*, 2018, **2018**, 1–11, DOI: 10.1155/2018/4854152.

10 J. H. Burton, T. D. Price, L. Cahue and L. E. Wright, The use of barium and strontium abundances in human skeletal tissues to determine their geographic origins, *Int. J. Osteoarchaeol.*, 2003, **13**(1–2), 88–95, DOI: 10.1002/oa.661.

11 K. L. Rasmussen, G. Milner, L. Skytte, N. Lynnerup, J. L. Thomsen and J. L. Boldsen, Mapping diagenesis in archaeological human bones, *Heritage Sci.*, 2019, **7**(1), 41, DOI: 10.1186/s40494-019-0285-7.

12 J. Cárdenas-Escudero, D. Galán-Madruga and J. O. Cáceres, Laser-Induced Breakdown Spectroscopy as an Accurate Forensic Tool for Bone Classification and Individual Reassignment, *Appl. Spectrosc.*, 2025, **79**(2), 241–259, DOI: 10.1177/00037028241277897.

13 C. Stadlbauer, C. Reiter, B. Patzak, G. Stingeder and T. Prohaska, History of individuals of the 18th/19th centuries stored in bones, teeth, and hair analyzed by LA–ICP–MS—a step in attempts to confirm the authenticity of Mozart's skull, *Anal. Bioanal. Chem.*, 2007, **388**(3), 593–602, DOI: 10.1007/s00216-007-1266-3.

14 R. A. Rezk, A. H. Galmed, M. Abdelkreem, N. A. A. Ghany and M. A. Harith, Quantitative analysis of Cu and Co adsorbed on fish bones *via* laser-induced breakdown spectroscopy, *Opt. Laser Technol.*, 2016, **83**, 131–139, DOI: 10.1016/j.optlastec.2016.02.025.

15 A.-F. Maurer, P. Barrulas, A. Person, J. Mirão, C. Barrocas Dias, O. Boudouma and L. Segalen, Testing LA-ICP-MS analysis of archaeological bones with different diagenetic

3190 | *J. Anal. At. Spectrom.*, 2025, **40**, 3184–3191

This journal is © The Royal Society of Chemistry 2025

histories for paleodiet prospect, *Palaeogeogr., Palaeoclimatol., Palaeoecol.*, 2019, **534**, 109287, DOI: **10.1016/j.palaeo.2019.109287**.

16 M. Martinez and M. Baudelet, Calibration strategies for elemental analysis of biological samples by LA-ICP-MS and LIBS – A review, *Anal. Bioanal. Chem.*, 2020, **412**(1), 27–36, DOI: **10.1007/s00216-019-02195-1**.

17 R. Kane and P. X. Ma, Mimicking the nanostructure of bone matrix to regenerate bone, *Mater. Today*, 2013, **16**(11), 418–423, DOI: **10.1016/j.mattod.2013.11.001**.

18 S. R. Stock, The Mineral-Collagen Interface in Bone, *Calcif. Tissue Int.*, 2015, **97**(3), 262–280, DOI: **10.1007/s00223-015-9984-6**.

19 B. Chang and X. Liu, Osteon: Structure, Turnover, and Regeneration, *Tissue Eng., Part B*, 2022, **28**(2), 261–278, DOI: **10.1089/ten.TEB.2020.0322**.

20 P. H. Schlesinger, H. C. Blair, D. Beer Stolz, V. Riazanski, E. C. Ray, I. L. Tourkova and D. J. Nelson, Cellular and extracellular matrix of bone, with principles of synthesis and dependency of mineral deposition on cell membrane transport, *Am. J. Physiol. Cell Physiol.*, 2020, **318**(1), C111–c124, DOI: **10.1152/ajpcell.00120.2019**.

21 I. Cacciotti, Cationic and Anionic Substitutions in Hydroxyapatite, in *Handbook of Bioceramics and Biocomposites*, ed. I. V. Antoniac, Springer International Publishing, 2014, pp. 1–68.

22 A. Ressler, A. Žužić, I. Ivanišević, N. Kamboj and H. Ivanković, Ionic substituted hydroxyapatite for bone regeneration applications: A review, *Open Ceram.*, 2021, **6**, 100122, DOI: **10.1016/j.oceram.2021.100122**.

23 M. Martinez, C. Bayne, D. Aiello, M. Julian, R. Gaume and M. Baudelet, Multi-elemental matrix-matched calcium hydroxyapatite reference materials for laser ablation: Evaluation on teeth by laser-induced breakdown spectroscopy, *Spectrochim. Acta, Part B*, 2019, **159**, 105650, DOI: **10.1016/j.sab.2019.105650**.

24 A. Ugarte, N. Unceta, C. Pécheyran, M. A. Goicolea and R. J. Barrio, Development of matrix-matching hydroxyapatite calibration standards for quantitative multi-element LA-ICP-MS analysis: application to the dorsal spine of fish, *J. Anal. At. Spectrom.*, 2011, **26**(7), 1421–1427, DOI: **10.1039/C1JA10037H**.

25 M. Razavi, S. Hu and A. S. Thakor, A collagen based cryogel bioscaffold coated with nanostructured polydopamine as a platform for mesenchymal stem cell therapy, *J. Biomed. Mater. Res.*, 2018, **106**(8), 2213–2228, DOI: **10.1002/jbm.a.36428**.

26 P. Augat and S. Schorlemmer, The role of cortical bone and its microstructure in bone strength, *Age Ageing*, 2006, **35**(suppl_2), ii27–ii31, DOI: **10.1093/ageing/afl081**.

27 R. A. S. Fessi, J. V. Santoso, S. S. Sugiarto, C. P. Danudiningrat, I. Nirwana, A. Meizarini and A. Yuliati, Analysis of Characteristics of Cancellous Rib Freeze-Dried Bovine Bone as a Substitution Material, *J. Int. Dent. Med. Res.*, 2024, **17**(1), 104–109.

28 A.-N. Tzavellas, C. Katrilaka, N. Karipidou, M. Kanari, M. Pitou, G. Koliakos, A. Cheva, T. Choli-Papadopoulou,

A. Aggeli and E. Tsiridis, The "Forgotten" Hydroxyapatite Crystals in Regenerative Bone Tissue Engineering: A Critical Review, *Crystals*, 2024, **14**(5), 448.

29 L. M. Rodríguez-Lorenzo, J. N. Hart and K. A. Gross, Structural and Chemical Analysis of Well-Crystallized Hydroxyfluorapatites, *J. Phys. Chem. B*, 2003, **107**(33), 8316–8320, DOI: **10.1021/jp027556o**.

30 A. L. Patterson, The Scherrer Formula for X-Ray Particle Size Determination, *Phys. Rev.*, 1939, **56**(10), 978–982, DOI: **10.1103/PhysRev.56.978**.

31 S. A. Hassanzadeh-Tabrizi, Precise calculation of crystallite size of nanomaterials: A review, *J. Alloys Compd.*, 2023, **968**, 171914, DOI: **10.1016/j.jallcom.2023.171914**.

32 M. C. Chang and J. Tanaka, FT-IR study for hydroxyapatite/collagen nanocomposite cross-linked by glutaraldehyde, *Biomaterials*, 2002, **23**(24), 4811–4818, DOI: **10.1016/s0142-9612(02)00232-6**.

33 L. C. Mendes, G. L. Ribeiro and R. C. Marques, In Situ Hydroxyapatite Synthesis: Influence of Collagen on Its Structural and Morphological Characteristic, *Mater. Sci. Appl.*, 2012, **3**(8), 580–586, DOI: **10.4236/msa.2012.38083**.

34 R. Sripriya and R. Kumar, A Novel Enzymatic Method for Preparation and Characterization of Collagen Film from Swim Bladder of Fish Rohu (Labeo rohita), *Food Nutr. Sci.*, 2015, **6**(15), 1468–1478.

35 J. R. B. Nascimento, S. C. Sartoretto, A. T. N. N. Alves, C. F. A. B. Mourão, V. R. Martinez-Zelaya, M. J. Uzeda, J. M. Granjeiro, P. Montemezzi, M. D. Calasans-Maia and J. A. Calasans-Maia, In Vitro and In Vivo Evaluation of Nanostructured Biphasic Calcium Phosphate in Granules and Putty Configurations, *Int. J. Environ. Res. Public Health*, 2021, **18**(2), 533.

36 R. M. Coyte, J. S. Harkness and T. H. Darrah, The Abundance of Trace Elements in Human Bone Relative to Bone Type and Bone Pathology, *GeoHealth*, 2022, **6**(6), DOI: **10.1029/2021gh000556**.

37 J.-M. Mermet, Limit of quantitation in atomic spectrometry: An unambiguous concept?, *Spectrochim. Acta, Part B*, 2008, **63**(2), 166–182, DOI: **10.1016/j.sab.2007.11.029**.

38 G. S. Senesi, R. S. Harmon and R. R. Hark, Field-portable and handheld laser-induced breakdown spectroscopy: Historical review, current status and future prospects, *Spectrochim. Acta, Part B*, 2021, **175**, 106013, DOI: **10.1016/j.sab.2020.106013**.

39 T. E. Conley, C. Richardson, J. Pacheco, N. Dave, T. Jursa, S. Guazzetti, R. G. Lucchini, S. Fendorf, R. O. Ritchie and D. R. Smith, Bone manganese is a sensitive biomarker of ongoing elevated manganese exposure, but does not accumulate across the lifespan, *Environ. Res.*, 2022, **204**, 112355, DOI: **10.1016/j.envres.2021.112355**.

40 Z. Ballová, M. Janiga and R. Hančinský, Comparison of Element Concentrations (Ba, Mn, Pb, Sr, Zn) in the Bones and Teeth of Wild Ruminants from the West Carpathians and the Tian-Shan Mountains as Indicators of Air Pollution, *Atmosphere*, 2019, **10**(2), 64.

This journal is © The Royal Society of Chemistry 2025

J. Anal. At. Spectrom., 2025, **40**, 3184–3191 | 3191